Delft University of Technology

A micro graphene high temperature sensor with a single Si$_3$N$_4$ protective layer

Tang, Chenggang; Zeng, Simei; Hong, Hao; Fang, Yuan; Li, Yuning; Wang, Yuqiang; Zhu, Mingqiang; Sun, Jingye; Deng, Tao

Important note
To cite this publication, please use the final published version (if applicable).
Please check the document version above.

A micro graphene high temperature sensor with a single Si$_3$N$_4$ protective layer

Chenggang Tang [a], Simei Zeng [a], Hao Hong [b], Yuan Fang [a], Yuning Li [a], Yuqiang Wang [a], Mingqiang Zhu [a,*], Jingye Sun [a], Tao Deng [a,*]

[a] School of Electronic and Information Engineering, Beijing Jiaotong University, Beijing 100044, China
[b] Department of Microelectronics, Delft University of Technology, Delft 2628 CD, the Netherlands

ARTICLE INFO

ABSTRACT

Temperature sensors are widely used in industrial production, national defense and military fields. The traditional temperature sensors normally operate in a limited temperature range no more than 200 °C, which cannot be used for extreme high temperature detections. In this paper, a thermal protection method for the sensing graphene membrane is proposed and a graphene high temperature sensor has been fabricated and investigated. By growing a single silicon nitride (Si$_3$N$_4$) protective layer on top of graphene, our design not only solves the problem that graphene is easily oxidized at high temperature, but also prevents graphene from being polluted by impurities, which would lead to the degradation of graphene performance. We further explore the protective effect of Si$_3$N$_4$ layer with different thicknesses on the performance of the sensor. It has been found that the 400 nm Si$_3$N$_4$ protective layer gives the best protective capability. The sensor exhibits a positive temperature coefficient (PTC) from 50 to 600 °C and a maximal temperature coefficient of resistance (TCR) value of 0.29% °C^{-1} at 150 °C is achieved. It has been demonstrated that our graphene high temperature sensor with protective layer structure maintains good stability not only at high temperature up to 600 °C, but also over a long-period of time under room temperature. In short, the high temperature sensor possesses a wide temperature measurement range with micro dimensions, a relatively high TCR and a smaller thermal hysteresis. The thermal protection approach proposed in this paper provides a new idea for the fabrication of high temperature pressure sensor, which is expected to be applied in aerospace engines and oil wells, etc.

1. Introduction

Temperature sensors have been widely used in industrial manufacture, biomedical, environmental perception, national defense and military fields [1–3]. Traditional temperature sensors can be generally divided into pressure temperature sensors, resistance temperature detectors (RTDs), thermistors and thermocouples. These temperature sensors have the characteristics of simple structure, low cost and high measurement accuracy. However, they are capable for temperature measuring up to 200 °C, not suitable for extremely harsh environment, such as high temperature, high pressure or strong radiation. At present, even thermocouple and high fiber-optical temperature sensors are adopted for high temperature detections, they still show some disadvantages such as large volume and complex operation. In recent years, with the continuous development of micro/nanofabrication technology, Microelectromechanical Systems (MEMS) temperature sensors have

gradually attracted more attentions. MEMS sensors adopt nanomaterials as the temperature-sensitive unit, showing the unique merits of short response time, high resolution and broad measurement range [4,5]. Most importantly, the MEMS techniques enable the devices to be fabricated in large quantities. As one of the two-dimensional (2D) nanomaterials, graphene has excellent electrical properties [6–8], good tensile mechanical properties [9] and remarkable thermal properties [10,11], which makes it outstanding among normal and high temperature sensors.

The development of high temperature sensors depends on the technological innovation of temperature-sensitive materials. The carbon atoms inside graphene are connected in the sp^2 hybrid form, forming a regular hexagonal honeycomb structure. Due to the strong bond energy of the carbon six-membered ring, graphene is able to withstand a high temperature up to 2100 °C in a vacuum environment [12]. Theoretical and experimental results show that the thermal conductivity of
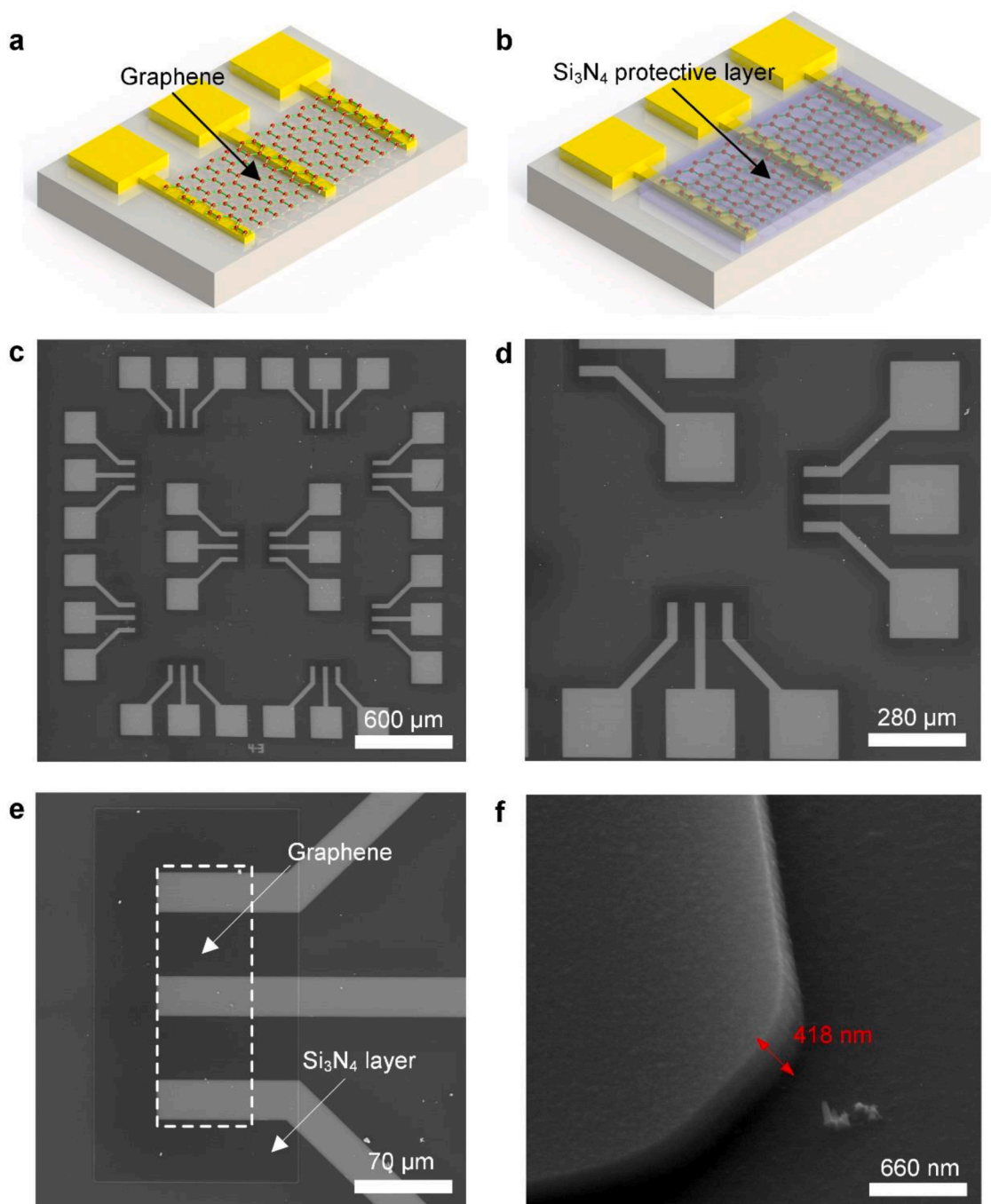

Fig. 1. The graphene high temperature sensors with a Si_3N_4 protective layer. (a) Transferring and patterning the monolayer graphene on top of electrodes. (b) Depositing top Si_3N_4 protective layer by PECVD and etching it by ICP. (c) Sensor array in a 1.5 cm×1.5 cm chip. (d) The zoomed-in view for the sensors. (e) Detailed view for the sensitive area of two sensors. (f) The oblique view for the Si_3N_4 protective layer.

monolayer graphene can reach to 5300 W/mK [13]. This value is much high than that of diamond (~2000 W/mK) [14] and carbon nanotubes (~3000 W/mK). The ultra-high thermal conductivity indicates an ultra-fast thermal response in the graphene based temperature sensors. In addition, graphene has large specific surface area (~ 2600 m^2/g) [15], which means a large thermal contact area compared to other materials. Moreover, graphene also has an extremely high carrier mobility, which fully ensures that the graphene temperature sensor shows sensitive response to temperature change. Recently, many researches on temperature sensors based on graphene have been published. Tran Thanh *et al.* fabricated a hybrid composite by coupling graphene with carbon nanotubes (CNT) using poly ionic liquid (PIL) as a

connector, showing a quick response to small temperature gradients [16]. Poonam *et al.* reported the sensing performance of reduced graphene oxide (rGO) resistive temperature sensors prepared with spin coatings. It has been found that the values of TCR and thermal hysteresis (H_{Th}) give significant differences in different temperature ranges [17]. Sun *et al.* used graphene-oxide (GO) hybrid as the sensing film to achieve a temperature measurement in air between 30 and 100 °C [18]. Li *et al.* employed BN/graphene/BN heterojunction as a sensitive material and found that there are two mechanisms for the change of graphene resistance caused by temperature change, which are thermal expansion effect and electron-phonon coupling effect [19].

Since graphene is only one-atom-thick, it is easily damaged without

protection. Furthermore, long-term exposure in the air will cause graphene adsorbs molecules or ions, such as O_2, N_2 and H_2O, leading to a failure performance [20,21]. Under high temperature environment, graphene would be oxidated by O_2 and disintegrated [22]. Therefore, the study on graphene protection is of significance for graphene devices under high temperature environment. Brenda *et al.* applied a self-assembled film of 1-aminodecane molecule as the passivation layer. The results show that the graphene was n-doped by the amino self-assembled film and the device had no obvious hysteretic with good stability [23]. Kim *et al.* used polymethylmethacrylate (PMMA)/ polybutadiene (PUB) bilayer polymer to protect graphene [24]. Sagade *et al.* deposited alumina on graphene field effect devices as a passivation layer by using atomic layer deposition (ALD). The device remained stable for several weeks when operated and stored in an open environment [25]. Su *et al.* used Si_3N_4 to encapsulate and protect graphene FET photoelectric sensors. Experimental results showed that graphene devices with a Si_3N_4 protective layer had low resistance fluctuation and were more stable in the open environment [26].

In this paper, graphene high temperature sensors were fabricated by depositing a certain thickness of Si_3N_4 protective layer on top of graphene. The sensor has a maximum tolerance temperature of 600 °C and a relatively high TCR. The electrical and thermal properties of the sensors with protective layers were studied. Meanwhile, the performances of the sensors with different thicknesses of Si_3N_4 protective layers were compared and contrasted. The resistance-temperature (RT) characteristic curves between 50 and 600 °C were also investigated. In addition, we explored the time stability of the sensors with and without the protective structure.

2. Experiments

The fabrication process for the graphene high temperature sensor encapsulated by protective layer structure is as follows. Firstly, the chromium (Cr)/platinum (Pt) metal electrodes were deposited on sapphire wafer by magnetron sputtering with thicknesses of 10 and 50 nm, respectively. Then, the monolayer CVD-grown graphene was transferred onto the small chips and patterned by oxygen plasma etching, shown in Fig. 1a. Finally, the Si_3N_4 protective layer with a thickness of 400 nm was deposited on top of graphene by plasma enhanced chemical vapor deposition (PECVD), and the electrodes were exposed by employing inductive coupled plasma (ICP) etching for subsequent testing, as shown in Fig. 1b. At this point, the fabrication of graphene high temperature sensor has been completed. More details for the fabrication processes can be found in Fig. S1 from the Supplementary Materials. The fabricated protective layer was utilized to protect graphene from environmental pollutions and oxidations at high temperatures.

The structure and surface morphology of graphene high temperature sensors were observed by optical microscope and environmental electron microscope (FEI Quanta 200 ESEM FEG). The peak values and position changes for graphene before and after heat treatment were analyzed by Raman spectroscopy (LabRam HR-800, Horiba Jobin Yvon). Then the electrical characteristics of the sensor with and without the protective layers were investigated by the semiconductor parameter analyzer (B1500A, Keysight) and probe station (Summit 12,000, Cascade). In order to explore the protective effect of the protective layers on graphene, the chips were placed into a Muffle furnace (TN-M1700). The *I-V* characteristic curves of the sensor were measured from room temperature to 600 °C. In addition, the resistance fluctuations for different devices after heat treatment were explored and the stability over time at high temperature were also investigated.

To explore the continuous resistance-temperature characteristics of our sensors, the 1.5 cm×1.5 cm chip was connected with a printed circuit board (PCB) via the gold wire bonding, pasted onto the upper and bottom ends of a high temperature resistant ceramic plate, respectively. The upper end of the ceramic plate (with chip) was placed into the furnace chamber through the furnace front open window for high
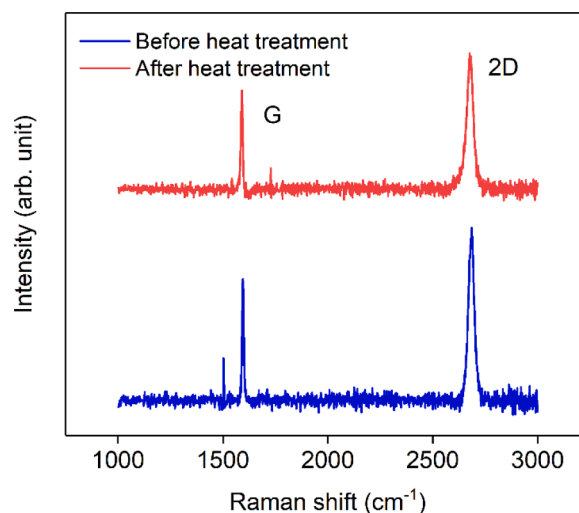

Fig. 2. Raman spectra of graphene high temperature sensor with Si_3N_4 protective layer before and after the heat treatment.

temperature treatment. The bottom end of the ceramic plate (with PCB) outside the furnace was connected to a digital multimeter to measure the real time resistance.

3. Results and discussions

The 4-inch wafer was sliced into 32 chips and each single 1.5 cm×1.5 cm chip contains 20 sensors as shown in Fig. 1c, where two sensors share one electrode in a unit. This design greatly reduces the chip area and proves the feasibility of large-scale fabrication. The zoomed-in view for the sensors and the detailed view for the sensitive area of the sensors are shown in Fig. 1d and e, respectively. The dimension of the sensitive area is only 80 μm×50 μm, showing the miniaturization characteristic. The graphene sensing film together with the protective layer were also illustrated in Fig. 1e.

Due to the transparency of the sapphire substrate, it is hardly to distinguish any difference between Si_3N_4 and graphene layers in the figure. But the presence of the graphene and protective Si_3N_4 layers would be confirmed by the Raman spectroscopy later. Fig. 1f shows the oblique view for the Si_3N_4 protective layer, with a measured thickness about 418 nm.

Raman spectroscopy was employed to characterize the graphene with the Si_3N_4 protective layer before and after the heat treatment, as shown in Fig. 2. Typical CVD-grown monolayer graphene shows three characteristic peaks, namely D peak (1350 cm^{-1}), G peak (1582 cm^{-1}) and 2D peak (2700 cm^{-1}). The intensity ratio of 2D to G (I_{2D}/I_G) is normally greater than 2 [27]. The D peak originates from the double resonant Raman-scattering process with the interaction between phonons and defects, such as in-plane substitution heteroatoms, vacancies, or grain boundaries/edges [28,29]. This peak is used to monitor the structural changes in graphene under high temperature in air. The smaller value of D peak implies a better thermal stability of graphene. It can be seen from Fig. 2 that D peak of the graphene with protective layer is not obvious before the heat treatment, indicating the fewer defects in graphene. 2D and G peaks were found at 2685.75 and 1594.44 cm^{-1}, respectively, with an intensity ratio of 1.42. Similar results were also observed and published in previous paper [30], due to the introduction of foreign atoms that break graphene's inherent lattice structure. After 90 s' annealing at 600 °C, the positions of 2D and G peaks slightly shift to 2676.28 and 1590.14 cm^{-1}, respectively, with an intensity ratio of 1.38. In addition, no obvious D peak is observed after the heat treatment, indicating that Si_3N_4 layer plays a significant role in thermal protection.

Fig. 3 shows the experimental results of electrical and thermal properties of the graphene high temperature sensors. The *I-V*
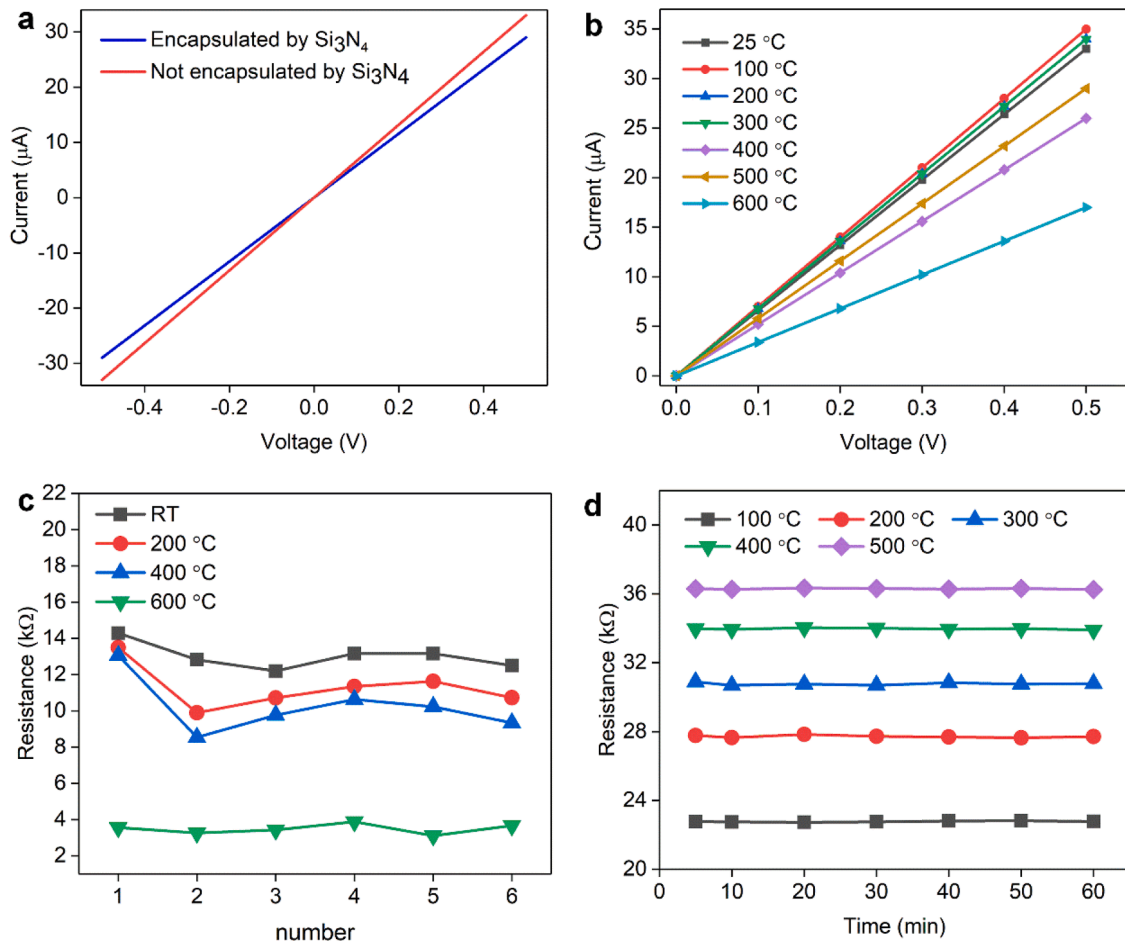
Fig. 3. The electrical and thermal properties of graphene high temperature sensors. (a) The *I-V* characteristic curve of the device with and without Si_3N_4 protective layer. (b) Thermal stability of graphene high temperature sensor between 25 and 600 °C. (c) The resistances of six randomly selected sensors under different temperatures. (d) Time stability of graphene high temperature sensor between 100 and 500 °C.

characteristic curves for the device with and without the Si_3N_4 protective layer at room temperature are shown in Fig. 3a. It can be found that the resistance of the device increases slightly with the Si_3N_4 protective layer, since the exposed graphene was p-doped by impurities, such as H_2O and O_2 in the air [20,21]. While, the addition of Si_3N_4 layer would n-dope the graphene, due to the amino group at the graphene/Si_3N_4 interface [31]. In order to explore the resistance-temperature characteristics, the sensor was placed into a Muffle furnace for 90 s at each interested temperature and taken out to cool down to room temperature. Fig. 3b shows the *I-V* characteristic curves for the sensors by varying the temperature from 25 to 600 °C. It can be clearly seen from the results that the device shows good stability under various temperatures. Si_3N_4 is a highly covalent compound and the self-diffusion coefficients of N and Si atoms are very small. The high density Si_3N_4 protective layer effectively insulates graphene from direct contact with oxygen at high temperatures. The measured resistances of six randomly selected sensors under different temperatures are shown in Fig. 3c. The resistance consistency φ is expressed as,

$$\varphi = \frac{\sigma}{\overline{R}} \times 100\% \tag{1}$$

$$\sigma^2 = \frac{\sum_{i=1}^{N}(R_i - \overline{R})^2}{N} \tag{2}$$

Where R_i is the resistance value of different sensors, $\overline{R}$ is the average resistance value, and N is the number of sensors. It has been calculated that the values of the resistance consistency φ under room temperature (RT), 200 °C, 400 °C, 600 °C are 5.53, 10.78, 14.85 and 8.10%,
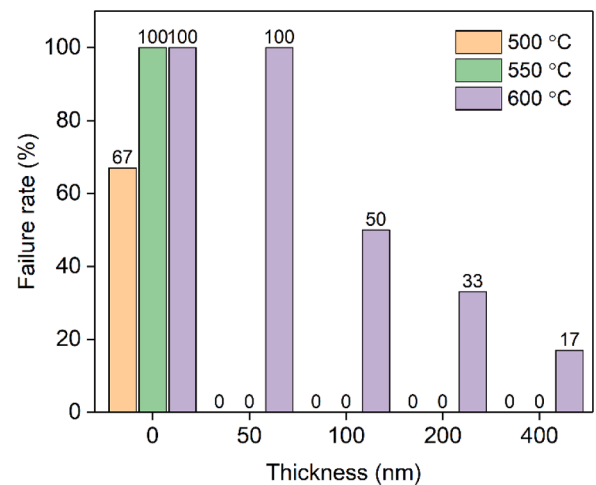

Fig. 4. Failure rate of graphene high temperature sensor with different thickness Si_3N_4 protective layer between 500 and 600 °C.

respectively, showing a good resistance consistency. Fig. 3d shows the measured resistance variation under different temperatures between 100 and 500 °C within one hour, where slight resistance fluctuation is seen and the maximum fluctuation is less than 0.44%, showing good high temperature stability.

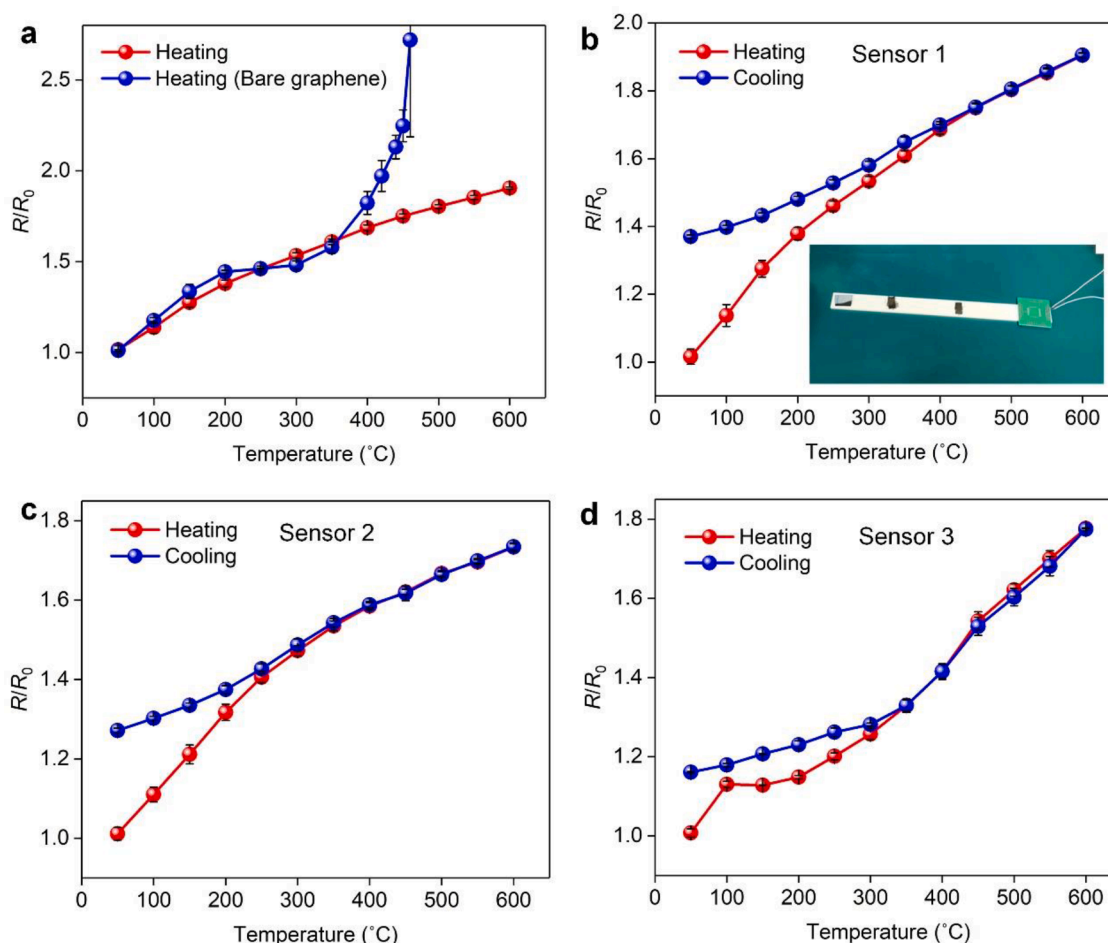The protective effect of Si_3N_4 protective layer with different

Fig. 5. (a) Comparison of the resistance-temperature output characteristic curves of the graphene high temperature sensors with and without protective layer. (b)-(d) The output characteristic curves of three different sensors from 50 to 600 °C with 50 °C interval. The experimental test device is also shown in the inset.

thicknesses on the devices are also explored. According to the fabrication process described previously, Si_3N_4 protective layers of 50, 100, 200 and 400 nm thicknesses were prepared respectively, while graphene high temperature sensors without protective layer were used as the control group. For each thickness, six sensors were randomly selected for 90 s heat treatment test under 500, 550 and 600 °C, and evaluated by the currents from the *I-V* characteristic curves, where a zero current means a failure. The failure rate is defined as,

$$\eta = \frac{D_{failure}}{D_{total}} \times 100\% \tag{3}$$

where D_{failure} and D_{total} are the numbers of failed and total devices. The experimental results are shown in Fig. 4. As the thickness of Si_3N_4 layer increases, the high temperature resistant of the devices are enhanced, and the failure rate of the device decreases. The failure rate of the device with 400 nm Si_3N_4 protective layer is only 17% at 600 °C. In the control group, all the graphene high temperature sensors without protective layer failed at 500 and 550 °C. Subsequent experiments for devices with 600 and 800 nm Si_3N_4 protective layers were also conducted and no significant reductions were detected in failure rates. In addition, the Si_3N_4 with a thickness of 1 μm appears to crack during the growth process, because the internal stress of Si_3N_4 is positively related to the thickness. Hence, 400 nm is the optimal thickness for the Si_3N_4 protective layer.

Fig. 5a shows the continuous resistance-temperature output characteristic curve of the sensor with and without the protective layer from 50 to 600 °C with 50 °C measured interval during the heating up process. The temperature of the furnace is controlled by a PID control program

with a 10 °C increment every one minute and three resistance values were recorded at each temperature point. It can be seen that the resistance of the device increases as temperature increases during the heating up process, showing a positive resistance temperature coefficient (PTC). The temperature coefficient of resistance (TCR) is expressed as,

$$TCR = \frac{R - R_0}{R_0 \Delta T} \tag{4}$$

where R and R_0 are the values of resistance at current and initial temperatures, ΔT is the difference between current and initial temperatures. The resistance of the sensor without protective layer increased rapidly at 400 °C and failed completely at 500 °C, as shown in Fig. 5a. This is attributed to the high temperature oxidation of graphene by oxygen. Fig. 5b–d show the output characteristic curve of three different sensors. The maximum TCR is calculated as 0.29%°C^{-1} at 150 °C from Fig. 5b. The temperature-sensitive properties of graphene are mainly affected by four mechanisms: electron-phonon coupling, graphene/substrate thermal expansion effect, intrinsic excitation and electron-charged particle interaction. In the process of temperature rises, the electric-phonon coupling and thermal expansion effect dominate. Meanwhile, the probability of electron scattering is improved and the carrier mobility is decreased, due to the enhancement in the lattice vibration. Since the thermal expansion coefficient of graphene differs from that of the sapphire substrate and the top Si_3N_4 layer, the thermal strain is formed within the graphene and the electrical conductivity is reduced, which is manifested as metal properties. In addition, it is detected from Fig. 5 that the heating up curve does not coincide with the cooling down curve, since the ceramic plate that supports the sensor shows very poor thermal
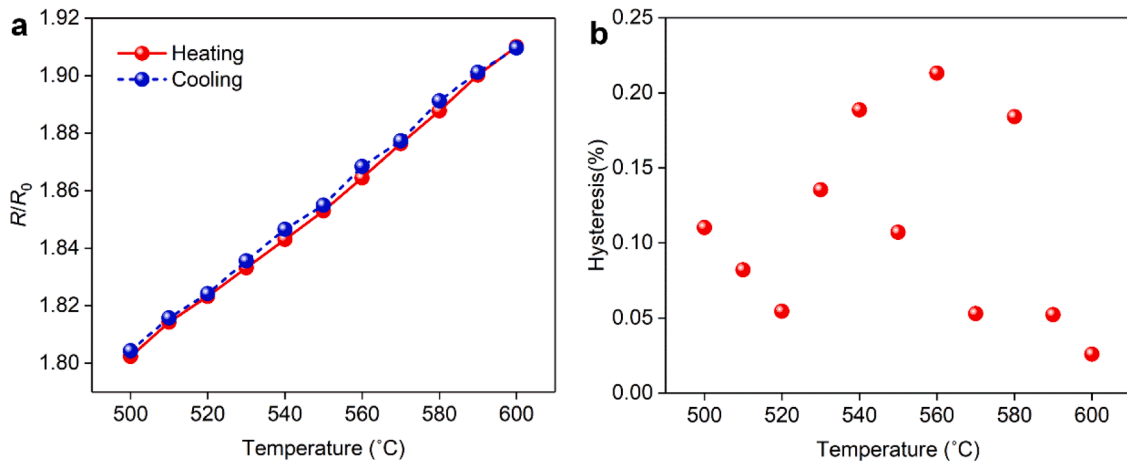
Fig. 6. (a) The output characteristic curve of the sensor from 500 to 600 °C with 10 °C interval. (b) The thermal hysteresis at different temperatures.

Table 1
Performance comparison among the temperature sensors.

Device structure	TCR (% °C^{-1})	Temperature range (°C)	Reference
Monolayer graphene with Si$_3$N$_4$ layer	0.29	RT~600	This work
BN/graphene/BN heterostructure	0.25	30~150	[19]
MWCNTs	0.068	30~100	[32]
3D GFET	0.41	30~150	[33]
CNT/PDMS	−0.23	40~80	[34]
Ag	0.223	20~60	[35]
Ni fibers	0.48	0~100	[36]

conductivity, causing a discrepancy between the furnace temperature and actual device temperature during the cooling down process. This experimental set-up would be improved by avoiding the contact between chip and plate in the future. After a long period of cooling, the resistance of the device can be restored to the initial value, indicating a good repeatability.

In order to give more details within the high temperature range, Fig. 6a shows the resistance-temperature characteristic curve of sensor 1 between 500 and 600 °C with 10 °C interval. It is observed that the curve reveals good linearity. The hysteresis is used to evaluate the repeatability, defined as,

$$Hysteresis(\%) = \frac{R_h - R_c}{R_h} \times 100 \tag{5}$$

where R_h and R_c are the resistance values at a specific temperature during the heating up and cooling down processes, respectively. Fig. 6b shows the thermal hysteresis of our sensor between 500 and 600 °C, where a maximum value of 0.21% was observed at 560 °C, indicating an excellent repeatability for high temperatures. Table 1 lists the key parameters for the performance of various types of temperature sensors. Among all the listed results, our sensors show the largest temperature range with high TCR.

In addition, the time stability of the device with the protective layer for 7 days and 3 months were investigated and compared with the original device, as shown in Fig. 7. The maximum resistance variances of the original device are 35 and 215% for 7 days and 3 months, while the maximum resistance variances of the Si$_3$N$_4$ encapsulated device are only 3.3 and 3.6%, respectively. The presence of Si$_3$N$_4$ protective layer would effectively prevent H$_2$O, O$_2$ and other impurities in the air from seriously contaminating graphene [20,21], enabling a long-term stability of the device.

4. Conclusion

In this paper, a graphene high temperature sensor with Si$_3$N$_4$ protective layer was fabricated and studied. The results show that the sensors have a good thermal stability up to 600 °C. It has been observed that
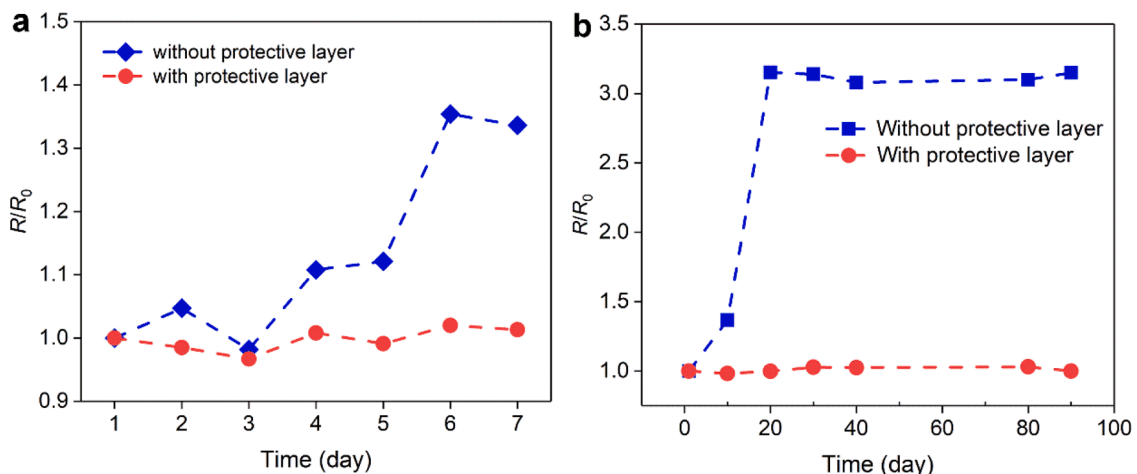

Fig. 7. Comparison of the long-term stabilities of the graphene high temperature sensors with and without protective layer for (a) 7 days and (b) 3 months.

that as the thickness of Si_3N_4 layer increases, the high temperature resistant of the sensors are enhanced. Furthermore, the sensor exhibits PTC between 50 and 600 ℃, and the maximal TCR is 0.29% ℃$^{-1}$. And a maximum thermal hysteresis value of only 0.21% is obtained between 500 and 600 ℃, showing a good repeatability. In addition, the resistance change rate of the device with protective layer is only 3.3% and 3.6% in 7 days and 3 months, showing long-term stability. By optimizing the thickness and growth technology of Si_3N_4, it is expected to achieve higher temperature sensing, opening a new way for the applications of graphene and other two-dimensional nanomaterials in the field of high temperature detections.

CRediT authorship contribution statement

Chenggang Tang: Investigation, Formal analysis, Writing – original draft, Writing – review & editing. **Simei Zeng:** Investigation, Data curation. **Hao Hong:** Methodology. **Yuan Fang:** Validation. **Yuning Li:** Formal analysis, Writing – review & editing. **Yuqiang Wang:** Visualization. **Mingqiang Zhu:** Validation, Supervision. **Jingye Sun:** Writing – original draft, Writing – review & editing, Project administration. **Tao Deng:** Conceptualization, Supervision, Writing – review & editing, Funding acquisition, Resources.

Declaration of Competing Interest

The authors declare the following financial interests/personal relationships which may be considered as potential competing interests:
Tao Deng reports was provided by the National Natural Science Foundation of China.

Acknowledgments

Supplementary materials

Supplementary material associated with this article can be found, in the online version, at doi:10.1016/j.surfin.2023.103029.

References

[1] G.S. Muneeb-ur-Rahman, A. Ullah, M.A. Zia-ur-Rahman, R. Khan, B.U. Zulfiqar, I. Ahmad, Resistive- and capacitive-type humidity and temperature sensors based on a novel caged nickel sulfide for environmental monitoring, J. Mater. Sci. Mater. Electron. 31 (2020) 3557–3563.

[2] Q. Lin, Z. Wu, N. Zhao, Z. Jiang, Q. Zhang, B. Tian, P. Shi, Design and numerical analysis of high-reflective film used in F-P sapphire optical fiber high-temperature sensor, Sens. Rev. 39 (2019) 162–170.

[3] C. Zhu, Y. Tang, J. Guo, R.E. Gerald, J. Huang, High-temperature and high-sensitivity pressure sensors based on microwave resonators, IEEE Sens. J. 21 (2021) 18781–18792.

[4] A.R.I. Ulinnuha, Z.A. Bahtiar, A.R. Nauri, I. Rhamadan, R.C. Wulansari, Z. Iqbal, The performance of the C12880MA MEMS sensor for classification of the roasting level of coffee bean, IOP Conf. Ser. Earth Environ. Sci. 924 (2021) 12021.

[5] Y. Nagarjuna, J. Lin, S. Wang, W. Hsiao, Y. Hsiao, AZO-based ZnO nanosheet MEMS sensor with different Al concentrations for enhanced H_2S gas sensing, Nanomaterials 11 (2021) 3377. Basel.

[6] A.K. Geim, K.S. Novoselov, The rise of graphene, Nat. Mater. 6 (2007) 183–191.

[7] K.I. Bolotin, K.J. Sikes, Z. Jiang, M. Klima, G. Fudenberg, J. Hone, P. Kim, H.L. Stormer, Ultrahigh electron mobility in suspended graphene, Solid State Commun. 146 (2008) 351–355.

[8] E.Y. Andrei, X. Du, I. Skachko, A. Barker, Approaching ballistic transport in suspended graphene, Nat. Nanotechnol. 3 (2008) 491–495.

[9] F. Liu, P. Ming, J. Li, Ab initio calculation of ideal strength and phonon instability of graphene under tension, Phys. Rev. B Condens. Matter Mater. Phys. 76 (2007), 064120.

[10] E. Pop, V. Varshney, A.K. Roy, Thermal properties of graphene: fundamentals and applications, MRS Bull. 37 (2012) 1273–1281.

[11] A.A. Balandin, Thermal properties of graphene and nanostructured carbon materials, Nat. Mater. 10 (2011) 569–581.

[12] Q. Shao, G. Liu, D. Teweldebrhan, A.A. Balandin, High-temperature quenching of electrical resistance in graphene interconnects, Appl. Phys. Lett. 92 (2008), 202108.

[13] A.A. Balandin, S. Ghosh, W. Bao, I. Calizo, D. Teweldebrhan, F. Miao, C.N. Lau, Superior thermal conductivity of single-layer graphene, Nano Lett. 8 (2008) 902–907.

[14] K. Mizuuchi, K. Inoue, Y. Agari, S. Yamada, M. Tanaka, M. Sugioka, T. Takeuchi, J. Tani, M. Kawahara, J.H. Lee, Y. Makino, Thermal properties of diamond-particle-dispersed Cu-matrix-composites fabricated by spark plasma sintering (SPS), Mater. Sci. Forum 638-642 (2010) 2115–2120.

[15] M.D. Stoller, S. Park, Y. Zhu, J. An, R.S. Ruoff, Graphene-based ultracapacitors, Nano Lett. 8 (2008) 3498–3502.

[16] T.T. Tung, C. Pham-Huu, I. Janowska, T. Kim, M. Castro, J. Feller, Hybrid films of graphene and carbon nanotubes for high performance chemical and temperature sensing applications, Small 11 (2015) 3485–3493.

[17] P. Sehrawat, S.S.I. Abid, P. Mishra, Reduced graphene oxide based temperature sensor: extraordinary performance governed by lattice dynamics assisted carrier transport, Sens. Actuators B 258 (2018) 424–435.

[18] P. Sun, M. Zhu, K. Wang, M. Zhong, J. Wei, D. Wu, H. Zhu, Small temperature coefficient of resistivity of graphene/graphene oxide hybrid membranes, ACS Appl. Mater. Interfaces 5 (2013) 9563–9571.

[19] M. Li, T. Zhang, P. Wang, M. Li, J. Wang, Z. Liu, Temperature characteristics of a pressure sensor based on BN/graphene/BN Heterostructure, Sensors 19 (2019) 2223. Basel.

[20] Z.G. Wang, Y.F. Chen, P.J. Li, X. Hao, Y. Fu, K. Chen, L.X. Huang, D. Liu, Effects of methane flux on structural and transport properties of CVD-grown graphene films, Vacuum 86 (2012) 895–898.

[21] C.G. Srivastava, L. Ci, L. Song, C. Rai, D. Jariwala, K.F. Kelly, P.M. Ajayan, Novel liquid precursor-based facile synthesis of large-area continuous, single, and few-layer graphene films, Chem. Mater. 22 (2010) 3457–3461.

[22] H.Y. Nan, Z.H. Ni, J. Wang, Z. Zafar, Z.X. Shi, Y.Y. Wang, The thermal stability of graphene in air investigated by Raman spectroscopy, J. Raman Spectrosc. 44 (2013) 1018–1021.

[23] B. Long, M. Manning, M. Burke, B.N. Szafranek, G. Visimberga, D. Thompson, J.C. Greer, I.M. Povey, J. MacHale, G. Lejosne, D. Neumaier, A.J. Quinn, Non-covalent functionalization of graphene using self-assembly of alkane-amines, Adv. Funct. Mater. 22 (2012) 717–725.

[24] H.H. Kim, Y. Chung, E. Lee, S.K. Lee, K. Cho, Water-free transfer method for CVD-grown graphene and its application to flexible air-stable graphene transistors, Adv. Mater. 26 (2014) 3213–3217.

[25] A.A. Sagade, D. Neumaier, D. Schall, M. Otto, A. Pesquera, A. Centeno, A.Z. Elorza, H. Kurz, Highly air stable passivation of graphene based field effect devices, Nanoscale 7 (2015) 3558–3564.

[26] F. Su, Z. Zhang, S. Li, P. Li, T. Deng, Long-term stability of photodetectors based on graphene field-effect transistors encapsulated with Si_3N_4 layers, Appl. Surf. Sci. 459 (2018) 164–170.

[27] A.C. Ferrari, J.C. Meyer, V. Scardaci, C. Casiraghi, M. Lazzeri, F. Mauri, S. Piscanec, D. Jiang, K.S. Novoselov, S. Roth, A.K. Geim, Raman spectrum of graphene and graphene layers, Phys. Rev. Lett. 97 (2006), 187401.

[28] Y. You, Z. Ni, T. Yu, Z. Shen, Edge chirality determination of graphene by Raman spectroscopy, Appl. Phys. Lett. 93 (2008), 163112.

[29] C. Neumann, L. Banszerus, M. Schmitz, S. Reichardt, J. Sonntag, T. Taniguchi, K. Watanabe, B. Beschoten, C. Stampfer, Line shape of the Raman 2D peak of graphene in van der Waals heterostructures, Phys. Status Solidi B 253 (2016) 2326–2330.

[30] D. Geng, S. Yang, Y. Zhang, J. Yang, J. Liu, R. Li, T. Sham, X. Sun, S. Ye, S. Knights, Nitrogen doping effects on the structure of graphene, Appl. Surf. Sci. 257 (2011) 9193–9198.

[31] Z. Wang, P. Li, Y. Chen, J. Liu, F. Qi, H. Tian, B. Zheng, J. Zhou, Air-stable n-type doping of graphene from overlying Si_3N_4 film, Appl. Surf. Sci. 307 (2014) 712–715.

[32] G. Liu, Q. Tan, H. Kou, L. Zhang, J. Wang, W. Lv, H. Dong, J. Xiong, A flexible temperature sensor based on reduced graphene oxide for robot skin used in internet of things, Sensors 18 (2018) 1400. Basel.

[33] Y. Fang, Y. Zhang, Y. Li, J. Sun, M. Zhu, T. Deng, A novel temperature sensor based on three-dimensional buried-gate graphene field effect transistor, Nanotechnology 32 (48) (2021), https://doi.org/10.1088/1361-6528/ac1f53.

[34] L. Wu, J. Qian, J. Peng, K. Wang, Z. Liu, T. Ma, Y. Zhou, G. Wang, S. Ye, Screen-printed flexible temperature sensor based on FG/CNT/PDMS composite with constant TCR, J. Mater. Sci. Mater. Electron. 30 (2019) 9593–9601.

[35] M.D. Dankoco, G.Y. Tesfay, E. Benevent, M. Bendahan, Temperature sensor realized by inkjet printing process on flexible substrate, Mater. Sci. Eng. B 205 (2016) 1–5.

[36] M. Husain, R. Kennon, Preliminary investigations into the development of textile based temperature sensor for healthcare applications, Fibers 1 (2013) 2–10.